



Essential Functions of MLL1 and MLL2 in Retinal Development and Cone Cell Maintenance

Chi Sun¹, Xiaodong Zhang¹, Philip A. Ruzycski¹ and Shiming Chen^{1,2*}

¹Department of Ophthalmology and Visual Sciences, St. Louis, MO, United States, ²Department of Developmental Biology, Washington University, St. Louis, MO, United States

OPEN ACCESS

Edited by:

Minzhong Yu,
Case Western Reserve University,
United States

Reviewed by:

Zi-Bing Jin,
Capital Medical University, China
Shuyi Chen,
Sun Yat-sen University, China
Vijay K. Jidigam,
Cleveland Clinic, United States

*Correspondence:

Shiming Chen
chenshiming@wustl.edu

Specialty section:

This article was submitted to
Cell Growth and Division,
a section of the journal
Frontiers in Cell and Developmental
Biology

Received: 05 December 2021

Accepted: 25 January 2022

Published: 09 February 2022

Citation:

Sun C, Zhang X, Ruzycski PA and
Chen S (2022) Essential Functions of
MLL1 and MLL2 in Retinal
Development and Cone
Cell Maintenance.
Front. Cell Dev. Biol. 10:829536.
doi: 10.3389/fcell.2022.829536

MLL1 (KMT2A) and MLL2 (KMT2B) are homologous members of the mixed-lineage leukemia (MLL) family of histone methyltransferases involved in epigenomic transcriptional regulation. Their sequence variants have been associated with neurological and psychological disorders, but little is known about their roles and mechanism of action in CNS development. Using mouse retina as a model, we previously reported MLL1's role in retinal neurogenesis and horizontal cell maintenance. Here we determine roles of MLL2 and MLL1/MLL2 together in retinal development using conditional knockout (CKO) mice. Deleting *Mll2* from Chx10+ retinal progenitors resulted in a similar phenotype as *Mll1* CKO, but removal of both alleles produced much more severe deficits than each single CKO: 1-month *double* CKO mutants displayed null light responses in electroretinogram; thin retinal layers, including shorter photoreceptor outer segments with impaired phototransduction gene expression; and reduced numbers of M-cones, horizontal and amacrine neurons, followed by fast retinal degeneration. Despite moderately reduced progenitor cell proliferation at P0, the neurogenic capacity was largely maintained in *double* CKO mutants. However, upregulated apoptosis and reactive gliosis were detected during postnatal retinal development. Finally, the removal of both MLLs in fated rods produced a normal phenotype, but the CKO in M-cones impaired M-cone function and survival, indicating both cell non-autonomous and autonomous mechanisms. Altogether, our results suggest that MLL1/MLL2 play redundant roles in maintaining specific retinal neurons after cell fate specification and are essential for establishing functional neural networks.

Keywords: MLL1 (KMT2A), MLL2 (KMT2B), conditional knockout, retinal development, functional maintenance, histone modifications, gene expression

INTRODUCTION

The mixed-lineage leukemia (MLL) family of histone lysine methyltransferases (KMTs) catalyze the methylation at lysine (K) 4 of histone H3 (Shilatifard, 2008; Crump and Milne, 2019). Their products, mono-, di- and tri-methylation of H3K4 are considered activating histone marks that are found at promoters of transcribed genes (Eissenberg and Shilatifard, 2010; Gu and Lee, 2013). The MLL family has six members, namely, MLL1 (KMT2A), MLL2 (KMT2B), MLL3 (KMT2C), MLL4 (KMT2D), SET1DA and SET1DB, all of which contain a conserved catalytic SET domain (Allis et al., 2007; Crump and Milne, 2019). These MLL enzymes usually form large multi-protein complexes (Yokoyama et al., 2004; Dou et al., 2006; Shinsky et al., 2015) that mediate chromatin remodeling and

transcriptional regulation during tissue genesis (Glaser et al., 2006; Krivtsov and Armstrong, 2007; Slany, 2016; Cenik and Shilatifard, 2021). MLL1/MLL2 form a distinct macromolecular complex (Sze and Shilatifard, 2016; Crump and Milne, 2019) found in many cell types of the central nervous system (CNS) (Jakovcevski et al., 2015; Kerimoglu et al., 2017; Brightman et al., 2018). Human mutations in MLL1 (KMT2A) and MLL2 (KMT2B) have been associated with cancer and syndromic neurological and psychiatric disorders, such as dystonia, intellectual disability and autism with variable age onsets (Jones et al., 2012; Meyers et al., 2017). However, their functions and mechanisms of action in the CNS development and neuronal disease pathogenesis remain to be elucidated.

The retina is the tissue of the CNS specialized for the vision sensation. It consists of conserved and well-characterized neuronal cell types, making it an ideal model for studying MLL functions in neurogenesis, neural network formation and maintenance. Retinal cells are organized into a multi-laminar structure in a mature retina (Young, 1985; Cepko et al., 1996; Bassett and Wallace, 2012; Cepko, 2014). The outer nuclear layer (ONL) contains rod and cone photoreceptor cells, where the light signal is converted into the neuronal signal. The inner nuclear layer (INL) hosts neurons of horizontal (HC), bipolar (BC) and amacrine cells (AC), as well as Müller glia (MG). The ganglion cell layer (GCL) contains retinal ganglion cells (GC) innervating to the brain. Synaptic connections between these layers form two additional layers known as the inner (IPL) and outer plexiform layers (OPL). Cell-type specification of the retina is largely conserved across vertebrate species (Austin and Cepko, 1995; Livesey and Cepko, 2001; Stenkamp, 2015; Wu et al., 2018; Lu et al., 2020). In mice, GC, cone photoreceptors and HC are fated in the first wave of cell birth during prenatal retinal neurogenesis, followed by the later birth waves of AC, rod photoreceptors, BC and MG during postnatal days (P) 0 to P5 (Young, 1985; Turner et al., 1990; Hafner et al., 2012; Emerson et al., 2013; Cepko, 2014). After cell fate specification, neuronal differentiation and synaptogenesis begin to establish connections between rod/cone primary neurons and secondary/tertiary neurons. By the end of 3 weeks, a functional neural network is established to mediate visual signal transmission and processing (Blanks et al., 1974; Tian, 2004; Soto et al., 2012; Guido, 2018; Furukawa et al., 2020; Szatko et al., 2020).

Retinal cell fate specification and differentiation are regulated by a network of transcription factors (TF) (Hennig et al., 2008; Swaroop et al., 2010; Mellough et al., 2019). CHX10 (also known as VSX2) is one of the earliest expressed TFs in the presumptive neural retina, and is required for retinal progenitor cell (RPC) proliferation and neurogenesis (Liu et al., 1994; Burmeister et al., 1996; Green et al., 2003; Livne-bar et al., 2006). CHX10 is also required for bipolar cell specification at a later development stage (Kim et al., 2008; Morrow et al., 2008). OTX2 is essential for establishing the photoreceptor lineage (Nishida et al., 2003; Koike et al., 2007) by inducing the expression of CRX, an OTX-like TF required for photoreceptor development and maintenance (Chen et al., 1997; Furukawa et al., 1997; Hennig et al., 2008). TFs acting downstream of OTX2/CRX govern photoreceptor specification, including NRL (Mears et al., 2001) for rods, THRB2 (Roberts

et al., 2006) and RXRG (Roberts et al., 2005) for cones, specifically in mouse, for short-wavelength (S) and medium-wavelength (M) cones. TFs required for the development of INL and GCL neurons include *Onecut1* (OC1) and *PROX1* for horizontal cells (Dyer et al., 2003; Wu et al., 2013), *PAX6* for amacrine cells (Remez et al., 2017), and *POU4F1* (*BRN3A*) for ganglion cells (Nadal-Nicolás et al., 2009).

In order to express specific genes in a given cell type, the chromatin at these gene loci must be configured to allow access by the transcription machinery. Specific TFs can regulate local chromatin remodeling during the retinal development by recruiting co-activators and histone modification enzymes at target genes (Li et al., 2007; Zhang et al., 2015). For example, CRX is required for the postnatal developing photoreceptors to gain DNA accessibility and write active histone marks H3K4me3 and H3K27Ac at photoreceptor gene loci (Ruzycski et al., 2018), which is important for the transcription cascade and visual function.

We previously reported, using conditional knockout mice, that MLL1 plays essential roles in regulating retinal progenitor cell proliferation, maintenance of horizontal neurons and formation of functional synapses between photoreceptors and inner neurons (Brightman et al., 2018). Here we aimed to unveil the roles of MLL2 and MLL1/MLL2 together in the development and maintenance of retinal neurons by characterizing the phenotypes of retina-specific knockout of *Mll2* and both *Mll1* and *Mll2*. We found that during the functional development, two MLLs played redundant roles in maintaining the retinal structure and function of photoreceptors and three types of inner retinal neurons. Both cell autonomous and non-autonomous functions contributed to cone/rod maintenance. These results implicated complex mechanisms of action of MLL1 and MLL2 in the retinal development and maintenance.

MATERIALS AND METHODS

Transgenic Mouse Lines

All mice in this study were on the genetic background of *C57BL/6J* (the Jackson Laboratory, Stock No: 000664) free of *rd1* and *rd8* mutations. The *Cre*, *Mll1 flox*, *Mll2 flox* mouse lines were obtained from various published colonies (Le et al., 2004; Rowan and Cepko, 2004; Glaser et al., 2006; Gan et al., 2010; Brightman et al., 2016). Both male and female mice were used in experiments.

All animal procedures were conducted according to the Guide for the Care and Use of Laboratory Animals of the National Institute of Health, and were approved by the Washington University in St. Louis Institutional Animal Care and Use Committee.

Western Blot

Each bio-replicate contained 2 retinæ from P0 or 1MO individual samples. Nuclear extract of each bio-replicate was obtained using NE-PER Nuclear and Cytoplasmic Extraction Reagents (ThermoFisher Scientific) and boiled at 100°C for 10 min. 15 µl of 2 µg/µl protein samples were loaded to 4–12%

SDS-PAGE gel, along with the Chameleon Duo Pre-stained Protein Ladder (LI-COR Biosciences), and run at 100 V for 1.5 h. Protein samples were transferred from the gel to a nitrocellulose membrane using Bolt™ Transfer (ThermoFisher Scientific) at 10 V for 2 h. Blocking was done with Intercept® (PBS) Blocking Buffer (LI-SOR Biosciences) for 2 h. Blotting was done with iBind Western Device (ThermoFisher Scientific) overnight according to the manufacturer's protocol. MLL1 and MLL2 antibodies were diluted 1:500, and HDAC1 antibody was diluted 1:1,000. IRDye® 680RD anti-rabbit secondary antibody was diluted 1:2000 (LI-COR Biosciences). All the imaging steps were performed with the Odyssey DLx Imaging System (LI-COR Biosciences).

Histology and Immunohistochemistry

Eyes were enucleated at various ages with the superior/dorsal side marked on the cornea, and fixed in 4% paraformaldehyde at 4°C overnight for paraffin embedded sections. Each retinal cross-section was cut 5 microns thick on a microtome. Hematoxylin and Eosin (H&E) staining was performed to examine retinal morphology. For IHC staining, sections firstly went through antigen retrieval with citrate buffer, and blocked with a blocking buffer of 5% donkey serum, 1% BSA, 0.1% Triton-x-100 in 1X PBS (pH-7.4) for 1 h. Sections were then incubated with primary antibodies at 4°C overnight. Sections were washed with 1X PBS containing 0.01% TritonX-100 (PBST) for 30 min, and then incubated with specific secondary antibodies for 1 h. Primary and secondary antibodies (**Supplementary Table S1**) were applied with optimal dilution ratios. All slides were mounted with hard set mounting medium with DAPI (Vectashield, Vector Laboratories, Inc., CA).

For IHC staining of retinal cryo-sections, eyes were fixed in 4% paraformaldehyde after the removal of lens for 1 h. Eyes were then immersed in increasing concentrations of phosphate-buffered sucrose solutions, and incubated overnight at 4°C in 20% phosphate-buffered sucrose solution. Eyes were incubated in a 1:1 mixture of OCT (optimal cutting temperature; Sakura Finetek) and 20% phosphate-buffered sucrose for 1 h. Eyes were embedded in OCT and snap frozen. Blocks were sectioned at 5 µm. Blocking and antibody staining were processed as described above.

For IHC staining of whole flat-mount retinæ, eyes were fixed in 4% paraformaldehyde for at least 6 h. Retinæ were dissected and blocked in the blocking buffer for 2 h. Retinæ were incubated with primary antibodies at 4°C overnight, followed by 1X PBST wash for 10 min, and then incubated with secondary antibodies for 3 h. Upon a final 1X PBST wash for 10 min, retinæ were placed flat on slides. All images were taken on a Leica DB5500 microscope. All images were acquired at 1000 µm from ONH for ≥ P14 samples and at 500 µm from ONH for P0 samples.

EdU Labeling

Edu labeling was performed with the Click-iT EdU Assay Kit (Invitrogen, ThermoFisher Scientific). Mice were IP injected with 10 µl of 10 mM Edu per gram mouse weight at P0. Eyes were fixed and paraffin embedded with procedures described above. EdU staining was done according to the manufacturer's protocol. IHC

staining was done prior to EdU staining for experiments involved both steps.

Morphometry and Cell Count Analysis

Thickness of retinal layers were measured on the H&E images at specific locations from the optical nerve head. Results of measurements were plotted in a spider graph. For cell counting analysis, numbers of fluorescent objects were tallied in the entire cross-section. At least 4 biological replicates of each genotype were used in the statistical analysis. Two-way ANOVA with multiple comparisons or Student's t-test were performed with $p < 0.05$, CI:95% using Graphpad Prism 8 (GraphPad Software, CA).

Electroretinogram

Whole animal ERGs were performed on 1- and 2-month-old mice using UTAS-E3000 Visual Electrodiagnostic System with EM for Windows (LKC Technologies Inc., MD). Mice were dark-adapted overnight prior to the tests. The experimental procedures were adapted from the previously published study of our lab (Brightman et al., 2018). ERG responses of biological replicates were recorded, averaged and analyzed using Graphpad Prism 8 (GraphPad Software, CA). The mean peak amplitudes of dark-adapted A and B waves and light-adapted B waves were plotted against log values of light intensities ($\text{cd}^* \text{s}/\text{m}^2$). The statistical analysis was done by two-way ANOVA with multiple pairwise comparisons (Tukey's).

Quantitative PCR

Each RNA sample was extracted from 2 retinæ of a mouse using the NucleoSpin RNA Plus kit (Macherey-Nagel, PA). RNA concentrations were measured using a NanoDrop One spectrophotometer (ThermoFisher Scientific). 2 µg of RNA was used to produce cDNA using First Strand cDNA Synthesis kit (Roche, IN). Technical triplicates were run for each gene. Primers used in this study were listed in **Supplementary Table S2**. The reaction master mix consisted of EvaGreen polymerase (Bio-Rad Laboratories, CA), 1 µM primer mix, and diluted cDNA samples. Samples were run using a two-step 40-cycle protocol on a Bio-Rad CFX96 Thermal Cycler (Bio-Rad Laboratories, CA). Data were analyzed with QBase software (Biogazelle, Belgium). The statistical analysis was done by two-way ANOVA or Student's t-test with $p < 0.05$, CI:95% using Graphpad Prism 8.

Chip-Seq

Chromatin immunoprecipitation (ChIP) assay was performed using six pooled P14/P30 *Mill1^{o/2} KO*, or (*Chx10*) CreNeg control retinæ per sample as previously described (Tran et al., 2014). Each sample was dissected and chromatin was cross-linked with 1% formaldehyde in PBS for 10 min at room temperature. After cross-linked cells were lysed and fragmented by sonication, chromatin fragments were immunoprecipitated with the antibodies to H3K4me3 (Millipore Sigma, Burlington, MA; 07-473), bound to Protein A/G PLUS-Agarose (Santa Cruz Biotechnology, SC2003). After extensive washing, the immunoprecipitated chromatin was eluted with 50 mM

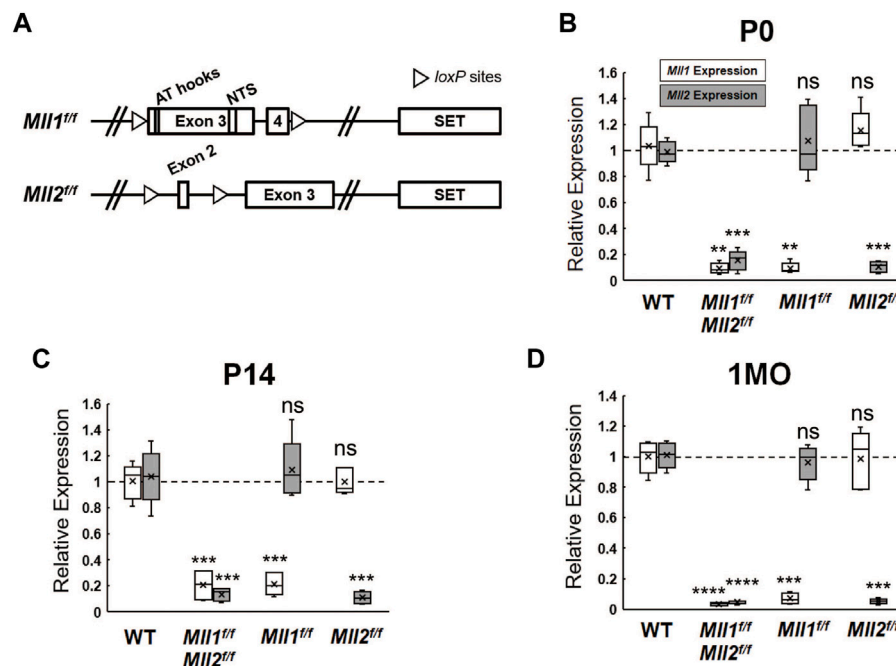


FIGURE 1 | *Mll1* and *Mll2* expression in conditional-knockout retinæ. **(A)** Diagrams of wide-type *Mll1* and *Mll2* genes indicating the positions of SET domains, motifs and *loxP* sites. Cre recombinase-mediated *Mll1* knockout removes exons 3 and 4 which encode the motifs of AT hooks and nuclear targeting signals (NTS) (Gan et al., 2010). Cre recombinase-mediated *Mll2* knockout removes exon 2 and invokes a frameshift in the mRNA (Glaser et al., 2006). **(B–D)** qRT-PCR analysis of *Mll1* and *Mll2* expression in P0, P14 and 1 month-old (1MO) mutant retinæ. Results are plotted as relative expression to *Chx10Cre⁻* littermate controls ($n = 5$). Asterisks (**, ***, ****) denote $p \leq 0.01$, $p \leq 0.001$, $p \leq 0.0001$ respectively by one-way ANOVA with Tukey's multiple comparisons, and ns means not significant.

NaHCO₃ 1% SDS, heated to 67°C to reverse the cross-links, and the DNA purified by ethanol precipitation. Libraries were prepared using the DNA SMART ChIP-Seq Kit (Clontech, Mountain View, CA). 10 ng of ChIP DNA was used as input for each sample. Libraries were sequenced on the Illumina NovaSeq6000 2 × 150 bp. Reads were trimmed using Trim Galore (v0.6.7) before mapping to mm9 genome build using Bowtie (v2.4.1). Duplicates were removed and alignments cleaned for proper alignments pairs using Picard (v2.25.7) and Samtools (v1.9.4). Peaks were called using the broad option in MACS2 (v2.1.1), merged using BEDTools (v2.27) merge function, and overlapping reads within each library were quantified using BEDTools coverage function. Enrichment was compared between genotypes using EdgeR (v3.30.3) and plotting performed in R using psych (v2.1.6) and ComplexHeatmap (v2.4.3) packages. Data from Aldiri et al. (GSE87064) was processed in same manner as above.

RESULTS

Generation of *Mll1* and *Mll2* Conditional Knockouts in Mouse Retinæ

Mll1 and *Mll2* are ubiquitously expressed in the developing mouse retinæ according to the published single-cell RNA-seq data (Clark et al., 2019) (Supplementary Figures S1A,B). Due to the embryonic lethality of *Mll1* or *Mll2* deficiency, we

utilized *Cre-LoxP*-mediated conditional knockout (CKO) to eliminate the function of each gene individually or simultaneously in selected retinal cell types. Cre excision produced a non-functional MLL1 protein lacking the nuclear targeting signals (NTS) (Gan et al., 2010) and/or a short non-functional MLL2 peptide resulted from a frameshift at exon 2 (Glaser et al., 2006) (Figure 1A). To investigate the roles of MLL1 and MLL2 in retinal neurogenesis, we crossed *Mll1^{f/f}* and/or *Mll2^{f/f}* mice to *Chx10-Cre-iresGFP* (Rowan and Cepko, 2004) mice, which expressed Cre recombinase in retinal progenitor cells. To confirm the success of Cre-mediated excision, we performed quantitative RT-PCR (qRT-PCR) analysis to determine *Mll1* and *Mll2* transcript levels in the mutant retinæ at postnatal day P0, P14, and 1 month (1MO) (Figures 1B–D). Detectable transcript levels of *Mll1* and *Mll2* were significantly reduced in *Chx10Cre⁺Mll1^{f/f}Mll2^{f/f}* (double CKO) retinæ at all tested ages as compared to *Chx10Cre⁻* (*CreNeg*) samples with the lowest level seen at 1MO. Likewise, MLL1 and MLL2 proteins were not detected in P0 double CKO retinæ by Western blotting (Supplementary Figure S1C). Notably, at all tested ages, reduction of *Mll1* or *Mll2* transcript levels in the double CKO retinæ was comparable to the corresponding single CKO. Furthermore, in either case of single CKO retinæ, no increase in the transcript level of the counterpart *Mll* gene was detected, suggesting no compensatory effect between *Mll1* and *Mll2* expression in single CKO retinæ.

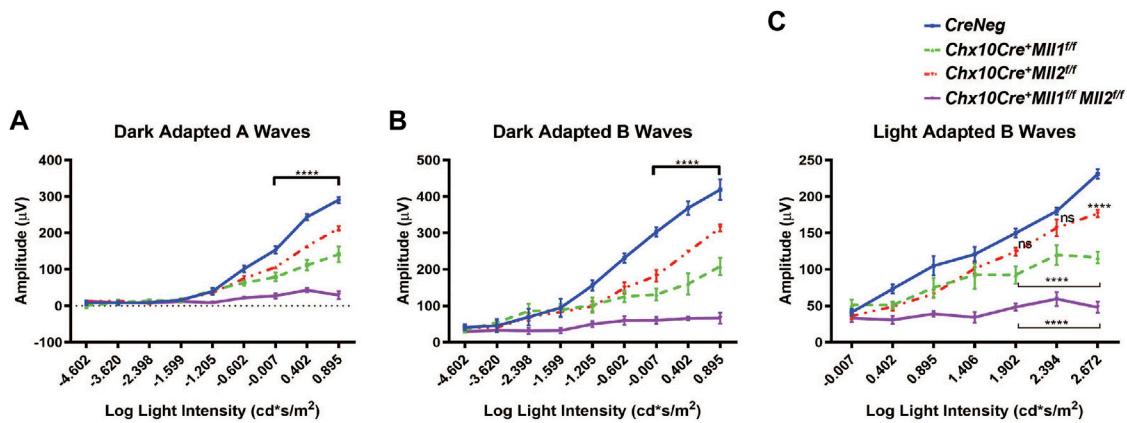


FIGURE 2 | Impaired retinal function of *Mll* mutants at 1MO. **(A)** Dark adapted A-wave electroretinogram (ERG) analysis of 1MO mice of the indicated genotypes. Mean amplitudes (μV) are plotted against stimulus light intensity. Error bars represent SEM ($n \geq 4$). **(B)** Dark adapted B-wave ERG analysis of 1MO mutant and control mice ($n \geq 4$). **(C)** Light adapted B-wave ERG analysis of 1MO mutant and control mice ($n \geq 4$). All statistics is done by two-way ANOVA and Tukey's multiple comparisons. Asterisks (****) denote $p \leq 0.0001$, and ns means not significant.

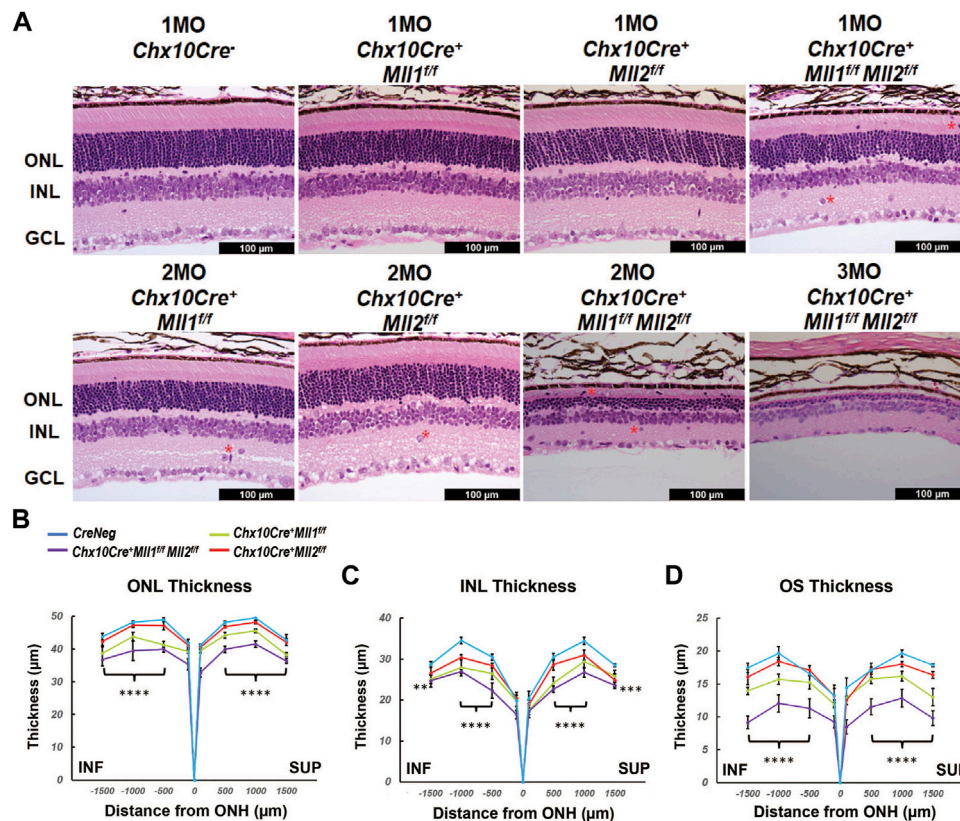


FIGURE 3 | Morphological defects of *Mll* mutants. **(A)** Hematoxylin and Eosin (H&E) cross-section staining of mature mutant and control retinas. Top panels show representative images of 1MO retinas of the indicated genotypes. Bottom panels show representative images of 2MO or 3MO retinas of the indicated genotypes. Red asterisks indicate mislocalized cells. ONL: outer nuclear layer; INL: inner nuclear layer; GCL: ganglion cell layer. Scale bar = 100 μm for all image panels. **(B)** ONL thickness (μm) in 1MO retinas at the indicated positions from the optic nerve head (ONH). SUP and INF indicate superior and inferior sides of the retina. Error bars represent mean (SD) ($n \geq 4$). **(C)** INL thickness in 1MO mutant and control retinas ($n \geq 4$). **(D)** Outer segment (OS) thickness in 1MO mutant and control retinas ($n \geq 4$). All statistics is done by two-way ANOVA and Tukey's multiple comparisons. Results of statistical analysis between the *double CKO* and *CreNeg* retinas are shown. Asterisks (**, ***, ****) denote $p \leq 0.01$, $p \leq 0.001$, $p \leq 0.0001$ respectively.

Mll1* and *Mll2* Deficiency Perturbs Retinal Function More Severely than Each Single *CKO

We performed electroretinography (ERG) to determine the effects of *Mll1* and *Mll2* deficiency on the retinal function. 1MO *double CKO* mutants showed no ERG responses in both dark-adapted (Figures 2A,B, purple line) and light-adapted (Figure 2C, purple line) conditions, indicating the absence of both rod- and cone-driven retinal function. In contrast, 1MO *single CKO* mutants produced detectable ERG responses (Figures 2A–C, red and green lines), but had significantly decreased A and B wave amplitudes at high light intensities as compared to those of *CreNeg* littermates. The ERG reductions were more pronounced in *Chx10Cre⁺Mll1^{fl/fl}* than in *Chx10Cre⁺Mll2^{fl/fl}* (Figures 2A–C, green line vs. red line). Similar patterns of ERG changes were also noticeable at 2MO (Supplementary Figure S2A). These results provided the first piece of evidence for distinct and redundant roles of MLL1/MLL2 in the development and maintenance of retinal function. Compound heterozygous mutants *Chx10Cre⁺Mll1^{WT/fl}Mll2^{fl/fl}* and *Chx10Cre⁺Mll1^{fl/fl}Mll2^{WT/fl}* showed similar ERG defects as those of the *single CKO* mutants (Supplementary Figures S2B,C) at 1MO and 2MO, indicating that at least one copy of *Mll1* or *Mll2* allele was essential for retinal function.

***Mll1* and *Mll2* Double *CKO* Mice Develop Thinner Retinae and Undergo Fast Retinal Degeneration in Young Adults**

To determine if the ERG defects in the mutant retinae were indicative of changes in the retinal structure and cellular morphology, we firstly examined the retinal cross-sections by hematoxylin-and-eosin (H&E) staining. At 1MO, all mutants displayed well-laminated neurons (Figure 3A). However, as compared to the *CreNeg* control, the *double CKO* retinae had significant reductions in overall retinal thickness, including ONL (Figure 3B), INL (Figure 3C), and outer segments (OS) of the photoreceptors (Figure 3D). Mislocalized cells were found (indicated by asterisks in Figure 3A) within the OS and IPL of the *double CKO* mutant. At 2MO, *single CKO* mice retained the laminated retinal morphology, despite a few mislocalized cells found at the IPL (Figure 3A, bottom left panels). In contrast, the *double CKO* retinae became much thinner than that at 1MO, suggesting severe degeneration and cell death (Figure 3A). By 3MO, both ONL and INL of the *double CKO* retinae degenerated further with only 1–2 rows of cells remaining in each layer (Figure 3A). Also, the OS length in the *double CKO* retinae was further reduced at 2MO and 3MO. Thus, loss of both *Mll1* and *Mll2* resulted in failure of morphological maintenance of the retinae, particularly affecting neuronal survival in the ONL and INL. Interestingly, 2MO compound heterozygous mutants, *Chx10Cre⁺Mll1^{WT/fl}Mll2^{fl/fl}* and *Chx10Cre⁺Mll1^{fl/fl}Mll2^{WT/fl}* appeared less affected in retinal morphology as compared to the double mutants (Supplementary Figure S3A), again suggesting at least one copy of either *Mll1* or *Mll2* allele was required for the maintenance of retinal integrity. At 6MO, *single*

CKO (Supplementary Figure S3B) and compound heterozygous mutants still maintained laminated retinal morphology, although ONL and INL appeared thinner than those of the control.

We next examined changes in the retinal morphology at early ages of postnatal development. No morphological or thickness abnormalities were found in the new-born P0 *double CKO* retinae (Supplementary Figures S4A,B). However, decreased ONL and INL thickness was found in P14 *double CKO* retinae as compared to *CreNeg* samples (Supplementary Figures S4C,D). These results suggested that *Mll1* and *Mll2* deficiency interfered with maintenance.

***Mll1* and *Mll2* Deficiency Induces Progressive Degeneration of M-Cones, Horizontal and Amacrine Cells**

To determine if *Mll1* and *Mll2* deficiency during the retinal development displayed cell-type specific effects, retinal cross-sections of 1MO mutants and controls were immunostained with cell-type specific markers. Given ERG deficits in the *double CKO* mutants, we firstly assessed the staining of rod and cone Opsins (Figures 4A–C). Rhodopsin (Rho) staining was correctly localized to the OS in the *double KO* retina (Figure 4A). However, consistent with the results of H&E staining (Figure 3D), the length of Rho + OS appeared shorter in the mutant than the *CreNeg* control (Figure 4A). Next, we stained for cone opsins. In mice, M and S cone subtypes were organized in dorsal-ventral counter-gradients, with M-opsin + cones predominantly found in the dorsal retina and S-opsin + cones in the ventral retina (Applebury et al., 2000). In the *double CKO* retinae, both M-opsin and S-opsin labeled cells were detected with the expected dorsal/ventral orientation (Figures 4B,C). However, while the number of M-opsin + cells was reduced to about 20% of the control, no significant reduction of S-opsin + cells was found (Figure 4H).

Next, we assessed changes of neuronal cell types in the inner retina. The *double CKO* retinae displayed significantly decreased numbers (10–30% remaining) of Calbindin + horizontal cells, and Calretinin + amacrine cells (Figures 4D,E,H). In contrast, the numbers of PKC α + rod-on bipolar cells (Figure 4D) and Brn3a + ganglion cells (Figure 4F) in mutants generally remained comparable to the controls (Figure 4H). Interestingly, 1MO *single CKO* retinae also had decreased numbers of M-cones, horizontal cells, and amacrine cells (Supplementary Figure S5), but the degree of reduction was less severe than that in the *double CKO* retinae. Taken together, the distinct and redundant roles of MLL1 and MLL2 were essential for the integrity of M-cones, horizontal cells, and amacrine cells.

We also examined the number and morphological features of Müller glia by glutamate synthetase (GS) staining. GS + Müller glia in the 1MO *double KO* retinae showed the typical cellular structure as compared to the control (Figure 4G), with cell bodies locating at the INL and endfeet terminating at the basal lamina. Mutant retinae also had similar numbers of Müller glia (Figure 4H), suggesting the development of these glial cells was generally unaffected in the mutants.

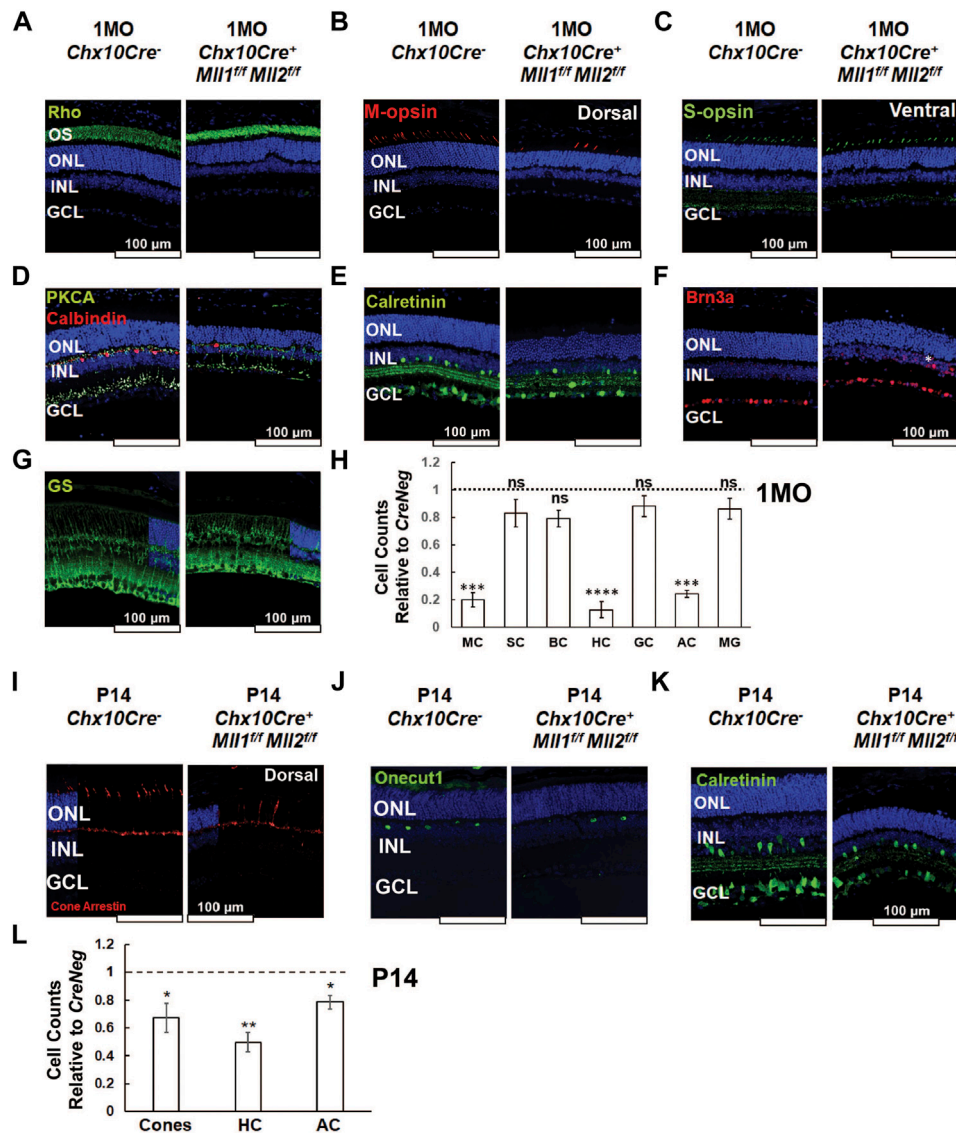
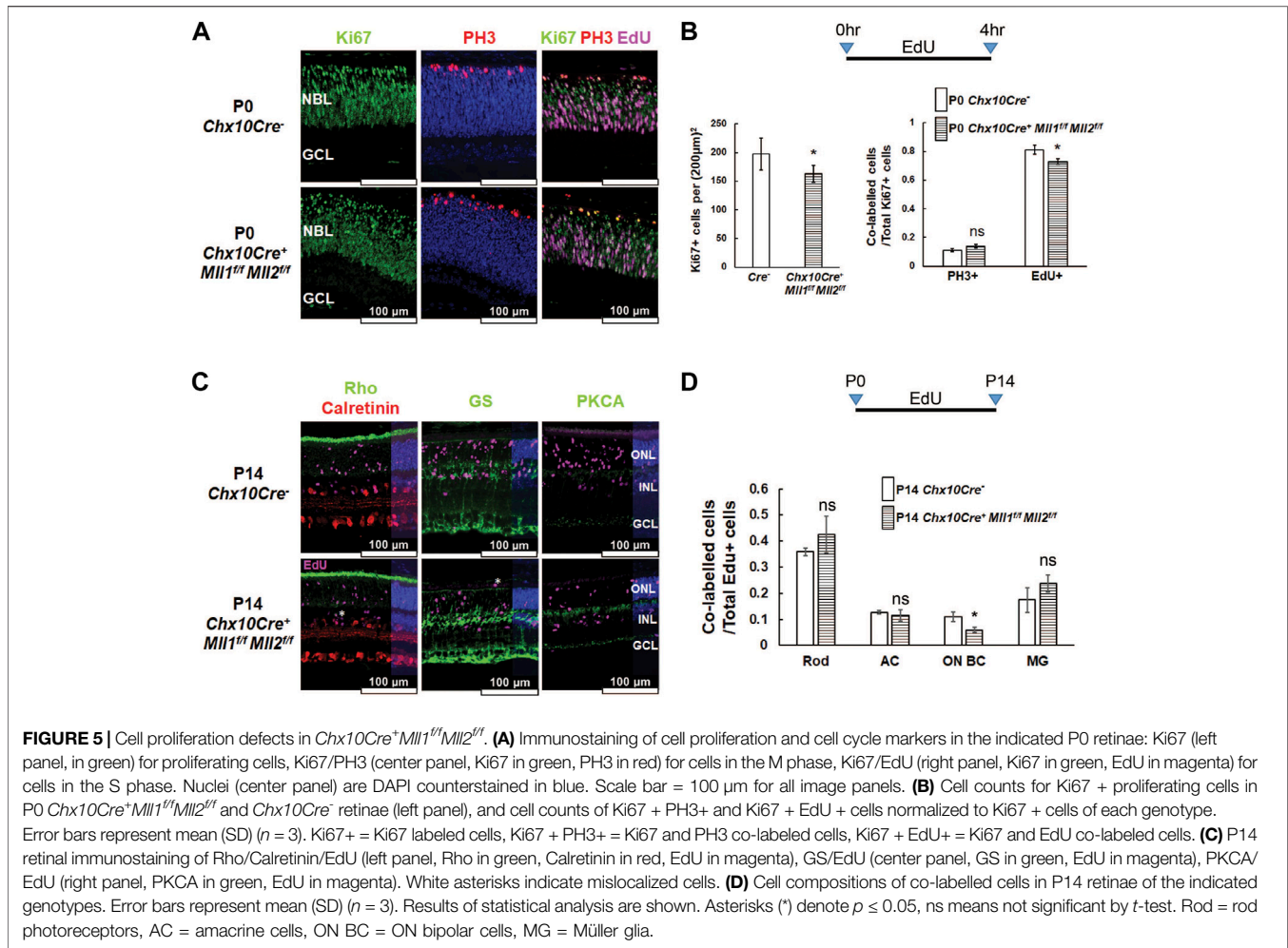


FIGURE 4 | Altered cell type composition in *Chx10Cre⁺Mll1^{fl/fl}Mll2^{fl/fl}* at 1MO and P14. **(A–G)** Immunostaining of the following cellular markers in 1MO retinas of the indicated genotypes: Rhodopsin (Rho, green in **A**) for rods, Medium-wave-sensitive opsin 1 (M-opsin, red in **B**) for M-cones, Short-wave-sensitive opsin 1 (S-opsin, green in **C**) for S-cones, Protein kinase C alpha (PKCA, green in **D**) for rod ON-bipolar cells, Calbindin D-28k (red in **E**) for ganglion cells, Calretinin (green in **F**) for amacrine and ganglion cells, and Glutamine synthetase (GS, green in **G**) for Müller glia. Asterisk indicated a mislocalized Brn3a + cell (**E**). **(H)** Cell counts for different retinal cell types in 1MO *Chx10Cre⁺Mll1^{fl/fl}Mll2^{fl/fl}* retinas, normalized to counts from *Chx10Cre⁻* (*CreNeg*) littermates. Error bars represent mean (SD) ($n \geq 3$). MC = M cone photoreceptors, SC = S cone photoreceptors, BC = bipolar cells, HC = horizontal cells, GC = retinal ganglion cells, AC = amacrine cells, MG = Müller glia. **(I–K)** Immunostaining of cellular markers in P14 retinas: Cone arrestin (red in **I**) for cones, Onecut1 (green in **J**) for horizontal cells, and Calretinin (green in **K**) for amacrine and retinal ganglion cells. **(L)** Cell counts for different retinal cell types in P14 *Chx10Cre⁺Mll1^{fl/fl}Mll2^{fl/fl}* retinas, normalized to counts from *Chx10Cre⁻* (*CreNeg*) littermates. Error bars represent mean (SD) ($n \geq 3$). Asterisks (*, **, ***, ****) denote $p \leq 0.05$, $p \leq 0.01$, $p \leq 0.001$, $p \leq 0.0001$ respectively, ns means not significant by *t*-test. Nuclei are counterstained by DAPI (blue). Scale bar = 100 μ m for all image panels.

To determine if the loss of selected retinal cell types was due to defective cell type specification or maintenance, we examined the early cell types in P0 retinas by immunostaining (**Supplementary Figure S6**). We used antibodies targeting Retinoid X Receptor Gamma (RXR γ) to label early fated cones at the apical retina, Onecut1 for early horizontal cells, Activating enhancer binding protein 2 alpha (AP2 α) for early amacrine cells, Paired box 6 (Pax6) for early amacrine and other neurons, and RBPMS and

Brn3a for ganglion cells (**Supplementary Figure S6A**). Cell count analysis showed that the numbers of these 4 cell types were comparable in the *double CKO* and *CreNeg* retinas (**Supplementary Figure S6B**), indicating that the production of early-born neurons was not severely affected in the *double CKO* retinas at P0.

We next analyzed the cell numbers of cones, horizontal and amacrine cells in mutant retinas at P14 when the cell fate



specification of all retinal neurons was completed (Figures 4I–K). The cell numbers of these cell types in mutants were lower than *CreNeg* samples (Figure 4L), but the degree of reduction at P14 (20–50%) was less than that at 1MO (80–90%), indicating a progressive loss of cones, horizontal and amacrine cells in the *double CKO* retinæ during the postnatal retinal development.

To determine if programmed cell death contributed to the loss of neurons, we immunostained mutant retinæ with activated caspase 3. At P0, a significant increase in the number of apoptotic cells (activated caspase 3+) were detected in mutant compared to *CreNeg* samples (Supplementary Figures S7A,B). Increased activated caspase 3 + cells were also notable at 1MO mutant retinæ, notably at INL (Supplementary Figure S7C). We also assessed the expression of pro- and anti-apoptotic genes. The transcript levels of the pro-apoptotic gene *Bcl-2-associated X (Bax)* were upregulated in P14 *double CKO* retinæ and more significantly in 1MO *double CKO* retinæ relative to the *CreNeg* control, while the expression of the anti-apoptotic gene *B-cell lymphoma 2 (Bcl2)* was insignificantly

reduced in mutants (Supplementary Figure S7D). These data suggested that in *double CKO* retinæ, the intrinsic apoptosis was initiated during the retinal development and accelerated at 1MO. This was consistent with retinal thinning and cell loss detected at P14 and 1MO, explaining the rapid degeneration afterwards.

To determine if *Mll1/Mll2* deficiency induced reactive gliosis, we performed immunostaining of Glial fibrillary acidic protein (GFAP) on retinal cross-sections of the *double CKO* mice. GFAP was the intermediate filament protein in retinal glia, its immunoreactivity indexed potential gliosis and correlation of neural damage. At 1MO, GFAP immunoreactivity was minimal in the control retinæ, but was drastically intensified in the *double CKO* retinæ (Supplementary Figure S8A), indicating severe reactive gliosis. The GFAP + reactive gliosis was lower in the *single CKO* retinæ than that in the *double CKO* retinæ. This high GFAP immunoreactivity in 1MO *double CKO* retinæ was confirmed by GFAP qRT-PCR (data not shown). The GFAP immunoreactivity was comparable in the P14 *double CKO* retinæ (Supplementary Figure S8B) to the control. Thus, the glial activation in mutants likely occurred after eye-opening,

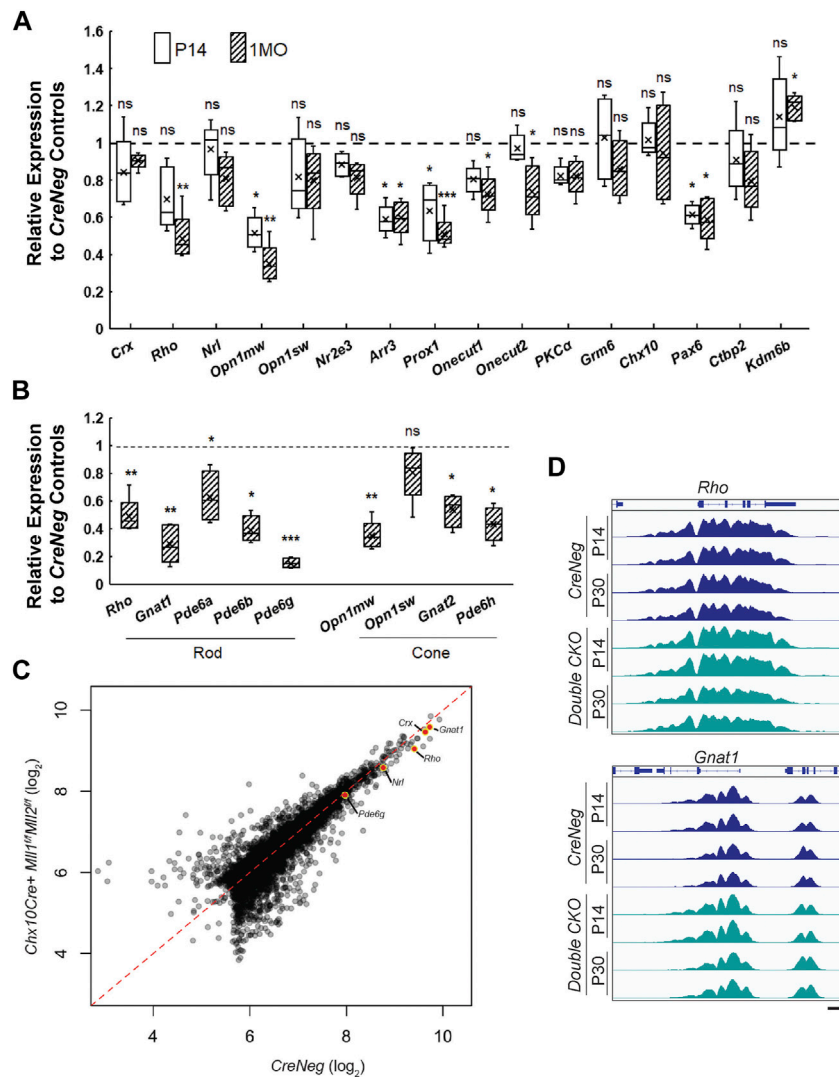


FIGURE 6 | Gene expression profile in P14 and 1MO $Chx10Cre^+Mll1^{fl/fl}Mll2^{fl/fl}$. **(A)** qRT-PCR analysis of selected genes in P14 and 1MO $Chx10Cre^+Mll1^{fl/fl}Mll2^{fl/fl}$ retinas. Results are plotted as relative expression to $Chx10Cre^-$ (*CreNeg*) littermate controls ($n \geq 4$). **(B)** qRT-PCR analysis of phototransduction gene expression in 1MO $Chx10Cre^+Mll1^{fl/fl}Mll2^{fl/fl}$ retinas. Results are plotted as relative expression to $Chx10Cre^-$ (*CreNeg*) littermate controls ($n \geq 4$). Asterisks (*, **, ***) denote $p \leq 0.05$, $p \leq 0.01$, $p \leq 0.001$ respectively by one-way ANOVA with Tukey's multiple comparisons, and ns means not significant. **(C)** Quantitative comparison of data from all H3K4me3 peaks in 1MO *CreNeg* and $Chx10Cre^+Mll1^{fl/fl}Mll2^{fl/fl}$ datasets. Promoter peaks of key phototransduction genes are highlighted. **(D)** ChIP-Seq data from P14 and 1MO $Chx10Cre^+Mll1^{fl/fl}Mll2^{fl/fl}$ and *CreNeg* retinas for H3K4me3 shows no differences at key rod phototransduction loci.

accompanied by the loss of retinal integrity at both structural and functional levels.

MLL1 and MLL2 Regulate Late Progenitor Cell Proliferation in Postnatal Developing Retina

Since cell proliferation defects were previously observed within P3 retinas of the $Chx10Cre^+Mll1^{fl/fl}$ mutants (Brightman et al., 2018), we sought to determine if a similar phenotype could be found in the *double CKO* retinas at an early postnatal age. We performed Ki67 immunostaining for proliferating cells in the retinal cross-sections of P0 samples (Figure 5A, left panel). The number of Ki67 +

proliferative cells in the *double CKO* retinas was significantly reduced (Figure 5B, left panel). We next examined if the cell cycle of Ki67 + proliferative cells was affected. Phospho-histone H3 (PH3) was used to label M-phase cells. PH3+ cells were found at the outer retinal neuroblast layer (NBL) of the *double CKO* and *CreNeg* retinas (Figure 5A, central panel). We did not find a significant difference in Ki67+ and PH3+ co-labelled cells between these samples (Figure 5B, right panel). To detect S-phase cells in P0 retinas, 5-Ethynyl-2'-deoxyuridine (EdU) was IP-injected into P0 mouse pups, and retinas were harvested 4 h later (Figure 5A, right panel). The *double CKO* retinas possessed fewer EdU + cells than *CreNeg* control (Supplementary Figures S9A,C). More importantly, the *double CKO* retinas had a decrease in the percentage of Ki67+/

EdU + co-labelled cells over the Ki67 + population (**Figure 5B**, right panel). These data suggested that *Mll1* and *Mll2* deficiency affected cell proliferation and cell cycle dynamics in P0 retinae, in particular, S-phase entry and M-phase exit.

To determine impacts of *Mll1* and *Mll2* deficiency on the production of specific cell types from late-born retinal progenitor cells (RPC), we performed EdU pulse-chase experiments. EdU-labeled P0 proliferating cells were assessed for specified cell-types at P14 (**Figures 5C,D**). Firstly, at P14, there were fewer EdU + cells in the *double CKO* retinae than in *CreNeg* controls (**Supplementary Figures S9B,C**). Secondly, the percentage of EdU co-labeled ON-bipolar cells in overall EdU-labeled cells was reduced about one half as compared to the control, but those of rods, late-born amacrine cells and Müller glia remained comparable (**Figures 5C,D**). These results suggested that, despite moderately reduced ON-bipolar cell production from P0 progenitor cells, overall, the intrinsic neurogenesis program was not severely compromised in the *double CKO* retinae.

***Mll1* and *Mll2* Deficiency Reduces the Expression of Phototransduction Genes Without Altering the Promoter Occupancy of the Active Histone Mark H3K4me3**

To unveil the molecular mechanisms for the cellular and functional defects in the *double CKO* retinae, we profiled specific gene expression changes at P14 and 1MO. qRT-PCR analysis showed there was a general trend toward reduced expression with tested transcripts in *double CKO* retinae as compared to the *CreNeg* retinae, suggesting that *Mll1/Mll2* deficiency had a negative impact on gene expression in general (**Figure 6A**). However, the transcript level of *lysine demethylase 6B (Kdm6b)* was slightly upregulated in 1MO *double CKO* retinae. The downregulation of the cell-type specific transcript levels supported the results of immunohistochemistry (**Figure 4**), further confirming cell composition changes at these two ages. In particular, this downregulation was most prominent in 3 cell types (**Figure 6A**), M-cones (*Opn1mw*, 30–50%), horizontal cells (*Prox1*, ~60%) and amacrine cells (*Pax6*, ~60%). Lastly, the changes in transcript expression at 1MO were more profound than those at P14, which was consistent with the progressive loss of the affected neurons. For example, the relative expression of *Opn1mw* was reduced from 52% at P14 to 34% at 1MO. The relative expression of *Rho* decreased from insignificant 70% at P14 to significant 48% at 1MO. These results, combined with the reduction of rod OS length at 1MO, suggested that rod cell integrity was affected before degeneration peaks. Additionally, we performed qRT-PCR with early-born cell markers at P0, including *Thrb* and *Rxrg* (cones), *Onecut1* (horizontal cells), *Chx10* and *Pax6*. No expression changes were detected in P0 *double CKO* retinae relative to the control (**Supplementary Figure S10**), suggesting that the programmed neurogenesis was unaffected by *Mll1/Mll2* deficiency.

We also examined gene expression of several other components in the rod and cone phototransduction cascades. qRT-PCR was performed to analyze transcripts of *G protein subunit alpha transducin 1 (Gnat1)*, *transducin 2 (Gnat2)*, *phosphodiesterase 6a*

(*Pde6a*), *6b (Pde6b)*, *6g (Pde6g)*, *6h (Pde6h)*. All tested genes besides *Pde6a* showed significant reduction in 1MO *double CKO* retinae (**Figure 6B**). Notably, the relative expression of *Gnat1* and *Pde6g* was decreased to 25 and 14% of the control, respectively. These results suggested that the rod and cone phototransduction cascade was disrupted in 1MO *double KO* retinae, providing an explanation for the lack of ERG responses. In contrast, the *single CKO* samples only had moderate or insignificant changes in gene expression (**Supplementary Figure S11**).

Since MLL1 and MLL2 function to methylate H3K4 at active gene promoters, we hypothesized that the gene misregulation in the mutants may be caused by the lack of the active histone mark H3K4me3 at photoreceptor specific promoters. We performed whole-retina chromatin immunoprecipitation sequencing (ChIP-Seq) to compare the *double CKO* mutants with *CreNeg* controls. Because rods represented 70% of all retinal cells, ChIP data represented a primarily rod signal in bulk ChIP-Seq analysis of P14 and 1MO samples (before severe rod degeneration in the mutants). Biological replicates displayed >98% concordance, indicating excellent reproducibility (**Supplementary Figure S12A**). Next, we compared the ChIP signal between mutants and controls and identified differentially enriched peaks at each age as well as those peaks that change over time in each model (**Supplementary Figure S12B**). To our surprise, there were only 279 peaks that displayed significant differences (>2 fold-change, $p < 0.05$) in these comparisons (**Figure 6C**). To understand the normal deposition of these histone modifications in retinal development, we analyzed the average change in signal over retinal development (E14-P21) (Aldiri et al., 2017). Peaks that were decreased in mutants generally showed consistent H3K4me3 across development, while peaks gained in mutants showed very little deposition of any active marks in the controls. We inspected the profiles of H3K4me3 at the rod genes that showed dramatic gene expression reductions (**Figure 6B**) but did not observe concordant reduction in the presence of H3K4me3 (**Figure 6D**). Together, these results suggested that *Mll1/Mll2* deficiency did not affect the remodeling of photoreceptor chromatin and the deposition of the H3K4me3 mark on promoters activated during cell type specification; other mechanisms must be responsible for the reduced expression of photoreceptor-specific genes.

MLL1 and MLL2 are Required for the Maintenance of Fated M-Cones, but not Rods

Although defective rod and cone phenotypes were seen in *Chx10-Cre*-mediated *double CKO* retinae, it was unclear if these phenotypes were stemmed from primary and/or secondary effects of *Mll1/Mll2* deficiency. To address this question, we determined cell autonomy by investigating the effects of *Mll1/Mll2* deficiency in fated rods and cones, respectively. To ablate *Mll1/Mll2* functions in fated rods, we crossed *Mll1^{fl/fl}Mll2^{fl/fl}* mice to *NrlCre* mice (Brightman et al., 2016), which began to express Cre recombinase in developing rods soon after rod cell specification and sustained Cre expression in adult rods. We also ablated *Mll1/Mll2* in fated M-cones by crossing *Mll1^{fl/fl}Mll2^{fl/fl}* mice to *MconeCre (HRGP-Cre)* mice (Le et al., 2004), which expressed Cre recombinase in M-opsin + cones beginning at early

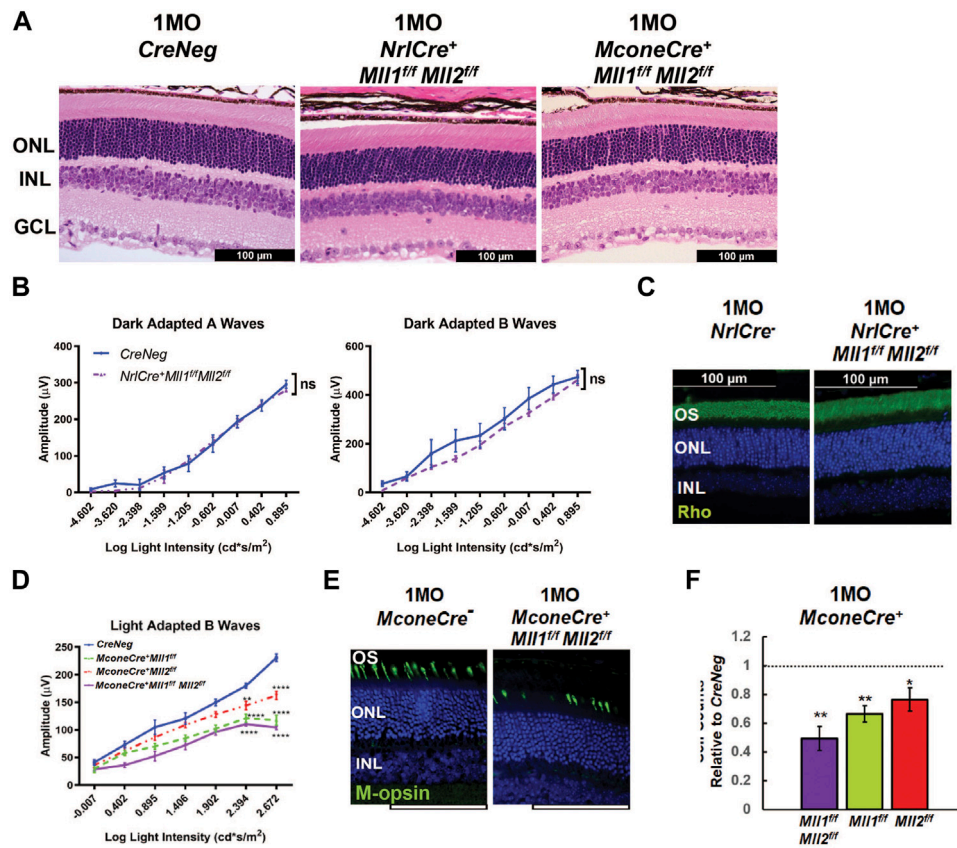


FIGURE 7 | Functional and morphological assessments of 1MO *NrlCre⁺Mll1^{fl/fl}Mll2^{fl/fl}* and *MconeCre⁺Mll1^{fl/fl}Mll2^{fl/fl}*. **(A)** H&E cross-section staining of 1MO *Cre⁻* (*CreNeg*, left panel), *NrlCre⁺Mll1^{fl/fl}Mll2^{fl/fl}* (center panel) *MconeCre⁺Mll1^{fl/fl}Mll2^{fl/fl}* (right panel) retinas. Scale bar = 100 μ m for all image panels. **(B)** Dark adapted A-wave (left) and Dark adapted B-wave (right) ERG analysis of 1MO *NrlCre⁺Mll1^{fl/fl}Mll2^{fl/fl}* and *Cre⁻* (*CreNeg*) mice. Mean amplitudes (μ V) are plotted against stimulus light intensity. Error bars represent SEM ($n \geq 4$). **(C)** Rho immunostaining in 1MO *NrlCre⁻* and *NrlCre⁺Mll1^{fl/fl}Mll2^{fl/fl}* retinas. **(D)** Light adapted B-wave ERG analysis of 1MO *MconeCre⁺Mll1^{fl/fl}Mll2^{fl/fl}*, *MconeCre⁺Mll1^{fl/fl}*, *MconeCre⁺Mll2^{fl/fl}*, and *Cre⁻* (*CreNeg*) mice. Mean amplitudes (μ V) are plotted against stimulus light intensity. Error bars represent SEM ($n \geq 4$). **(E)** M-opsin immunohistochemical staining in 1MO *MconeCre⁻* and *MconeCre⁺Mll1^{fl/fl}Mll2^{fl/fl}* dorsal retinas. **(F)** Cell counts for M cone photoreceptors in 1MO *MconeCre⁺Mll1^{fl/fl}Mll2^{fl/fl}*, *MconeCre⁺Mll1^{fl/fl}*, and *MconeCre⁺Mll2^{fl/fl}* retinas, normalized to counts from *MconeCre⁻* (*CreNeg*) littermates. Error bars represent mean (SD) ($n = 3$). All statistics is done by two-way ANOVA and Tukey's multiple comparisons. Asterisks (*, **, ***) denote $p \leq 0.05$, $p \leq 0.01$, $p \leq 0.001$ respectively, ns means not significant.

postnatal ages. H&E staining of 1MO *NrlCre⁺Mll1^{fl/fl}Mll2^{fl/fl}* and *MconeCre⁺Mll1^{fl/fl}Mll2^{fl/fl}* showed no apparent morphological abnormality (Figure 7A).

We next measured ERG responses in 1MO *NrlCre⁺Mll1^{fl/fl}Mll2^{fl/fl}* mice. No defects in dark-adapted A and B waves were detected in mutants compared to the controls (Figure 7B), and light-adapted ERG was also comparable (data not shown). Furthermore, Rho immunostaining showed no significant difference in OS morphology and thickness (Figure 7C). Transcript-level expression analysis of rod-enriched genes by qRT-PCR detected no changes in 1MO mutant retinas relative to the control (Supplementary Figure S13A). We did not detect any morphological and functional changes up to 6MO (data not shown). Collectively, these results suggested that *Mll1/Mll2* deficiency in developing and mature rods has limited impacts on cellular structure, function and survival. Thus, MLL1 and MLL2 functions were not required for the maintenance of fated rods.

By comparison, *MconeCre⁺Mll1^{fl/fl}Mll2^{fl/fl}* mice displayed cone functional and morphological defects. The amplitudes of light-adapted B waves of 1MO *MconeCre⁺Mll1^{fl/fl}Mll2^{fl/fl}* mice were significantly decreased as compared to controls (Figure 7D). 1MO *MconeCre⁺Mll1^{fl/fl}* and *MconeCre⁺Mll2^{fl/fl}* mice also showed decreased ERG responses as compared to controls, but were less severe than *MconeCre⁺Mll1^{fl/fl}Mll2^{fl/fl}* mice (Figure 7D). These results suggested that MLL1 and/or MLL2 were required for the functional maintenance of M-cones even after the cone differentiation.

We next performed immunostaining of Opn1mw (M-cones) together with PNA (all cones), or cone arrestin (Arr3) in retinal cross-sections of 1MO *MconeCre⁺Mll1^{fl/fl}*, *MconeCre⁺Mll2^{fl/fl}*, *MconeCre⁺Mll1^{fl/fl}Mll2^{fl/fl}* retinas (Figures 7E,F, Supplementary Figure S14). Quantification showed that the number of Opn1mw + cones in *MconeCre⁺Mll1^{fl/fl}Mll2^{fl/fl}* retinas was reduced to 50% of the control, while the numbers in *MconeCre⁺Mll1^{fl/fl}* or *MconeCre⁺Mll2^{fl/fl}* was down to only 70–80% (Figure 7F). To determine any spatial patterns associated with the cone number reduction, we performed

M-opsin and PNA co-staining on IMO whole-mount *MconeCre⁺ Mll1^{fl/fl} Mll2^{fl/fl}* retinæ (Supplementary Figure S15A). As expected, in IMO control samples, Opn1mw + cones were largely localized to the dorsal retina (Supplementary Figure S15A). By comparison, fewer Opn1mw + cones were found in the dorsal region of *MconeCre⁺ Mll1^{fl/fl} Mll2^{fl/fl}* retinæ (Supplementary Figure S15A). Cell count analysis showed that nearly half of Opn1mw+ (PNA+) cells were absent in the dorsal mutant retinæ, while the cone cell numbers were comparable in the ventral retinæ (Supplementary Figure S15B), confirming *Mll1/Mll2* deficiency in cones specifically affected M-cone integrity. qRT-PCR analysis showed significantly decreased expression of *Opn1mw* and *Arr3* in IMO *MconeCre⁺ Mll1^{fl/fl} Mll2^{fl/fl}* retinæ, but not in *MconeCre⁺ Mll1^{fl/fl}* or *MconeCre⁺ Mll2^{fl/fl}* retinæ (Supplementary Figures S13B,C), further confirming the immunostaining results. Taken together, these results described the cell autonomous effect of *Mll1/Mll2* deficiency on M-cone functional maintenance.

DISCUSSION

Redundant Roles of MLL1 and MLL2 in Retinal Development and Maintenance

MLL1 and MLL2 have been reported to play non-overlapping roles in development and cancer (Chen et al., 2017). In this manuscript, we used the conditional knockout strategy in mice to provide several pieces of evidence supporting that MLL1 and MLL2 redundant functions were required for the development and maintenance of neuronal function in the retina.

When MLL1 or MLL2 was removed from *Chx10* + retinal progenitor cells, similar phenotypic defects were observed, including moderately reduced photoreceptor responses to light stimuli (Figure 2, Supplementary Figure S2), loss of M-cones, horizontal and amacrine cells (Supplementary Figure S5). Thus, MLL1 and MLL2 essentially functioned in the indistinguishable regulatory pathways during retinal development and maintenance. MLL1 contributed more than MLL2 in each pathway, as all observed phenotypes were more severe in *Chx10Cre⁺ Mll1^{fl/fl}* than *Chx10Cre⁺ Mll2^{fl/fl}*. In each *single CKO* retinæ, there were no decreases or compensatory increases of transcript levels of the other *Mll* gene.

When both MLL1 and MLL2 were removed, all phenotypic defects found in the *single CKO* retinæ became much more severe. Notably, the *double CKO* mutants produced null ERG responses along with severely affected phototransduction gene expression (Figures 2, 6), massive reactive gliosis (Supplementary Figure S8) and apoptosis (Supplementary Figure S7) at IMO and rapid retinal degeneration after IMO (Figure 3). However, compound heterozygotes of *Mll1* and *Mll2* mutants produced significantly less severe ERG defects than the *double CKO* mutants, which was comparable to those in *single CKO* mutants (Supplementary Figures S2B,C). These results collectively confirmed that MLL1 contributed more than MLL2 in their redundant functions.

The functional redundancy between MLL1 and MLL2 was specific to this pair of MLLs. We previously reported that the *Mll1/Mll3 double CKO* retinæ produced a phenotype similar to that seen in

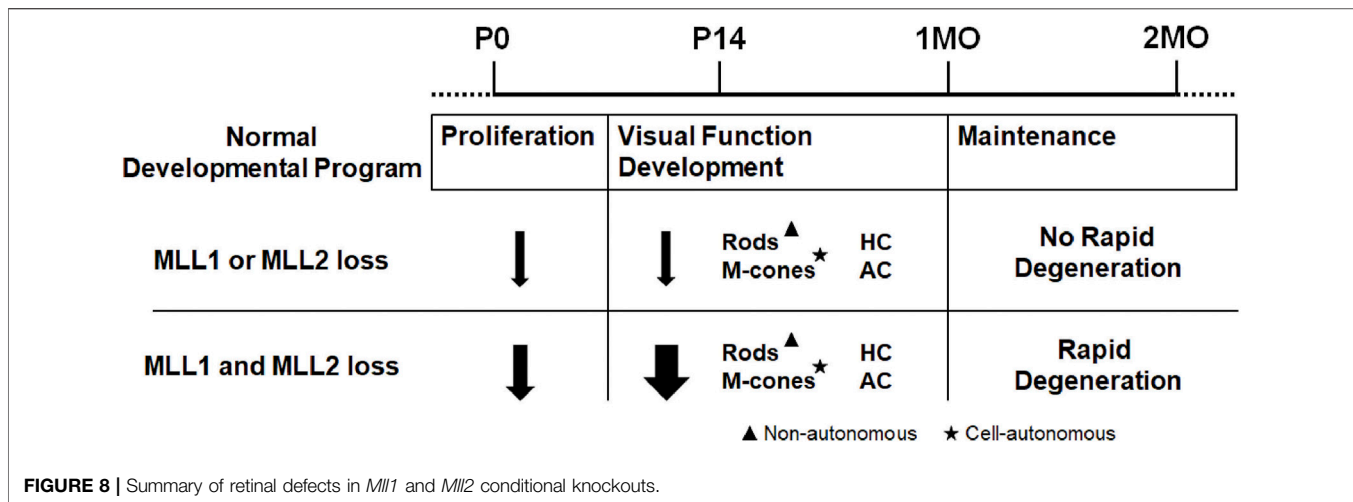
single Mll1 CKO retinæ (Brightman et al., 2018). MLL1 or MLL2 formed a complex distinct from those formed by other MLL family members, which provided a possible explanation for the redundant roles of MLL1 and MLL2. We proposed MLL1 and MLL2 acted together to regulate the neuronal proliferation, development and survival in the retina (Figure 8). Although we emphasized the redundant functions of MLL1 and MLL2 in this study, we did not rule out distinct functions of each gene, particularly for unique mechanisms of action at the molecular level. As an example, previous studies reported both MLL1 and MLL2 regulated *Hox* gene expression essential for body patterning during development, but they bound on distinct *Hox* loci with MLL1 on *HoxA* and *HoxC* and MLL2 on *HoxB* (Yu et al., 1995; Milne et al., 2002; Glaser et al., 2006). Future studies are needed to determine the molecular mechanisms underlining MLL1/MLL2 redundant functions in the retina, including their individual actions on specific neurons.

The Mechanisms Underlying Retina Layer Thinning and Functional Deficits in *Mll1/Mll2 Double CKO* Samples

One major phenotype of *Mll1/Mll2* deficiency was the thinning of retinal layers and the loss of specific types of neurons. In P0 *Chx10Cre⁺ Mll1^{fl/fl} Mll2^{fl/fl}* retinæ, the numbers of early-born neurons and expression levels of specific transcription factors were comparable to controls. Thus, the genesis and cell specification of the early-born neurons were normal. However, the development and maintenance of rods, M-cones, horizontal and amacrine cells were negatively affected at P14 and IMO (Figure 4), along with increased apoptosis throughout the first 4 weeks of postnatal development (Supplementary Figure S7).

Both cell autonomous and non-autonomous mechanisms were involved. The cellular mechanisms for the loss of rods were more complex, and likely involve cell non-autonomous (secondary) effects. Key observations included, firstly, the majority of rods survived between P14 to IMO with shorter segments. At IMO, apoptosis was apparent to cells at INL, not to ONL cells. Secondly, significant injury-induced reactive gliosis was present in the IMO *Chx10Cre⁺ Mll1^{fl/fl} Mll2^{fl/fl}* retinæ, correlating cellular stress in general. Lastly and most importantly, the removal of both *Mll1/Mll2* for developing rods (by *NrlCre*) did not produce rod functional deficits or cell loss. In addition, rod degeneration as secondary effects by neuronal loss at INL has been reported. For example, the loss of horizontal cells due to *Onecut1* and *Onecut2* TF deficiency induced subsequent rod degeneration (Sapkota et al., 2014).

In contrast, the M-cone phenotype was largely attributed to a cell autonomous mechanism, as M-cone defects was observed in retinæ with *Chx10-Cre* and *Mcone-Cre* mediated *Mll1/Mll2* deficiency. Notably, *Mll1/Mll2* deficiency only affected the M-cones, not S-cones. The mechanisms for such specificity of the MLL actions on cone subtypes remain to be determined. Further studies are needed to determine if protein factors regulating the S/M cone gradient or cone opsin expression are affected in the *double CKO* mutants.



Defects in neurogenesis may also contribute to retinal thinning and reduced cell numbers in INL of the *double CKO*, particularly during the first 2 weeks of postnatal development. P0 *Chx10Cre⁺Mll1^{fl/fl}Mll2^{fl/fl}* retinae had reduced number of Ki67+ and EdU + co-labelled cells, suggesting *Mll1* and *Mll2* collectively affect S-phase entry of retinal proliferating cells. This was consistent with published studies from mouse brain tissue and human cancer cell lines (Denissov et al., 2014; Jakovcevski et al., 2015; Chen et al., 2017; Kerimoglu et al., 2017). In our previous study, *Chx10Cre⁺Mll1^{fl/fl}* showed an insignificant decrease in S-phase cell number, while this study presented a further decline in the *double CKO* retinae, suggesting a potential redundancy of *Mll1* and *Mll2* in regulating S-phase entry of retinal progenitors. Our EdU pulse-chase experiments at P0 to P14 showed that after cell cycle exit, P0 progenitor cells in the *double CKO* retinae could produce all four types of late-born cells, namely, rods, ON-bipolar cells, amacrine cells and Muller glial. Together with the unchanged number of early-born neurons at P0, these results suggested that *Mll1* and *Mll2* did not regulate retinal cell-type specification. Although there was a reduction of ON-bipolar cells in EdU pulse-chase experiments from P0 to P14, the overall bipolar cell numbers were unchanged at 1MO. Further studies are required for examining the functions of MLLs in different windows of the retinal development.

1MO *Chx10Cre⁺Mll1^{fl/fl}Mll2^{fl/fl}* mutants displayed null ERG response, despite the presence of rows of ONL cells. One possible explanation was the loss of synaptic connections between photoreceptors and inner neurons. The presynaptic proteins Ctbp2/RIBEYE and VGLUT1 were present at the outer plexiform layer (**Supplementary Figure S16**) of the *double CKO* retinae, although we could not conclude if synaptic connections were functional. The most likely explanation was the decrease in phototransduction, based on two observations: 1) the absence of A-waves indicating no signals of ERG response, and 2) the downregulation of key rod and cone phototransduction genes. It was unclear if other mechanisms affecting phototransduction were involved.

It remains to be determined if gene misregulation in specific neurons of *Mll1/Mll2* deficient retinae is due to altered histone

H3 K4-methylation. We attempted to address this question by examining changes of rod-specific gene expression and chromatin occupancy of the H3K4me3 mark. Our surprising finding was that in spite of the downregulation of rod-specific genes, normal H3K4me3 signals were detected at the regulatory regions of these genes in *Chx10-Cre* mediated *Mll1/Mll2* knockouts. Instead, H3K4me3 changes were seen in the regulatory regions of constitutively expressed genes that were unknown to have rod-specific functions. Thus, both H3K4me3-dependent and independent mechanisms may attribute to the misregulation in rod functional development and maintenance. It is possible that the misregulation mechanisms involved in minor cell types, such as M-cones, horizontal and amacrine cells might be different from those of rods. Cell type-specific knockout and single cell-related approaches are needed to elucidate these mechanisms.

CONCLUSION

In conclusion, this study is the first kind to address the redundancy functions of MLLs in neuroretinal development and maintenance. Our findings highlight the complex functions of the MLL1 and MLL2 in neuronal cell types. Our findings may inform the pathogenesis of the syndromic neurological disorders associated with human *MLL1* and *MLL2* mutations and phenotype variability.

DATA AVAILABILITY STATEMENT

The datasets presented in this study can be found in online repositories. The names of the repository/repositories and accession number(s) can be found below: NCBI SRA; PRJNA778180.

ETHICS STATEMENT

The animal study was reviewed and approved by Washington University in St. Louis Institutional Animal Care and Use Committee.

AUTHOR CONTRIBUTIONS

SC conceived of the study, CS and SC designed the experiments, CS and XZ performed experiments, CS analyzed data, PR performed bioinformatics analyses of ChIP-Seq results, CS, PR, and SC wrote the manuscript. All authors read and approved the final manuscript.

FUNDING

Authors thank the funding of NIH grants EY012543 (to SC) and EY002687 (to WU-DOVS), and unrestricted funds from Research to Prevent Blindness (to WU-DOVS).

REFERENCES

- Aldiri, I., Xu, B., Wang, L., Chen, X., Hiler, D., Griffiths, L., et al. (2017). The Dynamic Epigenetic Landscape of the Retina during Development, Reprogramming, and Tumorigenesis. *Neuron* 94 (3), 550–568.e10. doi:10.1016/j.neuron.2017.04.022
- Allis, C. D., Berger, S. L., Cote, J., Dent, S., Jenuwien, T., Kouzarides, T., et al. (2007). New Nomenclature for Chromatin-Modifying Enzymes. *Cell* 131 (4), 633–636. doi:10.1016/j.cell.2007.10.039
- Applebury, M. L., Antoch, M. P., Baxter, L. C., Chun, L. L. Y., Falk, J. D., Farhangfar, F., et al. (2000). The Murine Cone Photoreceptor: A Single Cone Type Expresses Both S and M Opsins with Retinal Spatial Patterning. *Neuron* 27 (3), 513–523. doi:10.1016/S0896-6273(00)00062-3
- Austin, C. P., and Cepko, C. L. (1995). "Specification of Cell Fate in the Vertebrate Retina," in *Neural Cell Specification: Molecular Mechanisms and Neurotherapeutic Implications*. Editors B. H. J. Juurlink, P. H. Krone, W. M. Kulyk, V. M. K. Verge, and J. R. Doucette (Springer US), 139–143. doi:10.1007/978-1-4615-1929-4_11
- Bassett, E. A., and Wallace, V. A. (2012). Cell Fate Determination in the Vertebrate Retina. *Trends Neurosci.* 35 (9), 565–573. doi:10.1016/j.tins.2012.05.004
- Blanks, J. C., Adinolfi, A. M., and Lolley, R. N. (1974). Synaptogenesis in the Photoreceptor Terminal of the Mouse Retina. *J. Comp. Neurol.* 156 (1), 81–93. doi:10.1002/cne.901560107
- Brightman, D. S., Razafsky, D., Potter, C., Hodzic, D., and Chen, S. (2016). Nrl-Cretransgenic Mouse mediates loxP recombination in Developing Rod Photoreceptors. *genesis* 54 (3), 129–135. doi:10.1002/dvg.22918
- Brightman, D. S., Grant, R. L., Ruzycycki, P. A., Suzuki, R., Hennig, A. K., and Chen, S. (2018). MLL1 Is Essential for Retinal Neurogenesis and Horizontal Inner Neuron Integrity. *Sci. Rep.* 8 (1), 11902. doi:10.1038/s41598-018-30355-3
- Burmeister, M., Novak, J., Liang, M.-Y., Basu, S., Ploder, L., Hawes, N. L., et al. (1996). Ocular Retardation Mouse Caused by Chx10 Homeobox Null Allele: Impaired Retinal Progenitor Proliferation and Bipolar Cell Differentiation. *Nat. Genet.* 12 (4), 376–384. doi:10.1038/ng0496-376
- Cenik, B. K., and Shilatifard, A. (2021). COMPASS and SWI/SNF Complexes in Development and Disease. *Nat. Rev. Genet.* 22 (1), 38–58. doi:10.1038/s41576-020-0278-0
- Cepko, C. L., Austin, C. P., Yang, X., Alexiades, M., and Ezzeddine, D. (1996). Cell Fate Determination in the Vertebrate Retina. *Proc. Natl. Acad. Sci.* 93 (2), 589–595. Available at: <https://www.ncbi.nlm.nih.gov/pubmed/8570600>. doi:10.1073/pnas.93.2.589
- Cepko, C. (2014). Intrinsically Different Retinal Progenitor Cells Produce Specific Types of Progeny. *Nat. Rev. Neurosci.* 15 (9), 615–627. doi:10.1038/nrn3767
- Chen, S., Wang, Q.-L., Nie, Z., Sun, H., Lennon, G., Copeland, N. G., et al. (1997). Crx, a Novel Otx-like Paired-Homeodomain Protein, Binds to and Transactivates Photoreceptor Cell-Specific Genes. *Neuron* 19 (5), 1017–1030. doi:10.1016/s0896-6273(00)80394-3
- Chen, Y., Anastassiadis, K., Kranz, A., Stewart, A. F., Arndt, K., Waskow, C., et al. (2017). MLL2, Not MLL1, Plays a Major Role in Sustaining MLL-Rearranged

ACKNOWLEDGMENTS

Authors are grateful to Dr. Brian Clark for sharing single-cell RNA-seq data and analyzing *Mll1/Mll2* expression profiles; Mingyan Yang, Guangyi Ling and Belinda Dana for technical assistance; Dr. Patricia Ernst and Dr. Francis Stewart for providing *Mll1 flox* and *Mll2 flox* mice, respectively.

SUPPLEMENTARY MATERIAL

The Supplementary Material for this article can be found online at: <https://www.frontiersin.org/articles/10.3389/fcell.2022.829536/full#supplementary-material>

- Acute Myeloid Leukemia. *Cancer Cell* 31 (6), 755–770.e6. doi:10.1016/j.ccell.2017.05.002
- Clark, B. S., Stein-O'Brien, G. L., Shiau, F., Cannon, G. H., Davis-Marcisak, E., Sherman, T., et al. (2019). Single-Cell RNA-Seq Analysis of Retinal Development Identifies NFI Factors as Regulating Mitotic Exit and Late-Born Cell Specification. *Neuron* 102 (6), 1111–1126.e5. doi:10.1016/j.neuron.2019.04.010
- Crump, N. T., and Milne, T. A. (2019). Why Are So many MLL Lysine Methyltransferases Required for normal Mammalian Development? *Cell. Mol. Life Sci.* 76 (15), 2885–2898. doi:10.1007/s00018-019-03143-z
- Denissov, S., Hofemeister, H., Marks, H., Kranz, A., Ciotta, G., Singh, S., et al. (2014). Mll2 Is Required for H3K4 Trimethylation on Bivalent Promoters in Embryonic Stem Cells, whereas Mll1 Is Redundant. *Development* 141 (3), 526–537. doi:10.1242/dev.102681
- Dou, Y., Milne, T. A., Ruthenburg, A. J., Lee, S., Lee, J. W., Verdine, G. L., et al. (2006). Regulation of MLL1 H3K4 Methyltransferase Activity by its Core Components. *Nat. Struct. Mol. Biol.* 13 (8), 713–719. doi:10.1038/nsmb1128
- Dyer, M. A., Livesey, F. J., Cepko, C. L., and Oliver, G. (2003). Prox1 Function Controls Progenitor Cell Proliferation and Horizontal Cell Genesis in the Mammalian Retina. *Nat. Genet.* 34 (1), 53–58. doi:10.1038/ng1144
- Eissenberg, J. C., and Shilatifard, A. (2010). Histone H3 Lysine 4 (H3K4) Methylation in Development and Differentiation. *Dev. Biol.* 339 (2), 240–249. doi:10.1016/j.ydbio.2009.08.017
- Emerson, M. M., Surzenko, N., Goetz, J. J., Trimarchi, J., and Cepko, C. L. (2013). Otx2 and Onecut1 Promote the Fates of Cone Photoreceptors and Horizontal Cells and Repress Rod Photoreceptors. *Dev. Cell* 26 (1), 59–72. doi:10.1016/j.devcel.2013.06.005
- Furukawa, T., Morrow, E. M., and Cepko, C. L. (1997). Crx, a Novel Otx-like Homeobox Gene, Shows Photoreceptor-Specific Expression and Regulates Photoreceptor Differentiation. *Cell* 91 (4), 531–541. doi:10.1016/S0092-8674(00)80439-0
- Furukawa, T., Ueno, A., and Omori, Y. (2020). Molecular Mechanisms Underlying Selective Synapse Formation of Vertebrate Retinal Photoreceptor Cells. *Cell. Mol. Life Sci.* 77 (7), 1251–1266. doi:10.1007/s00018-019-03324-w
- Gan, T., Jude, C. D., Zaffuto, K., and Ernst, P. (2010). Developmentally Induced Mll1 Loss Reveals Defects in Postnatal Haematopoiesis. *Leukemia* 24 (10), 1732–1741. doi:10.1038/leu.2010.171
- Glaser, S., Schaft, J., Lubitz, S., Vintersten, K., van der Hoeven, F., Tuffeland, K. R., et al. (2006). Multiple Epigenetic Maintenance Factors Implicated by the Loss of Mll2 in Mouse Development. *Development* 133 (8), 1423–1432. doi:10.1242/dev.02302
- Green, E. S., Stubbs, J. L., and Levine, E. M. (2003). Genetic rescue of Cell Number in a Mouse Model of Microphthalmia: interactions between Chx10 and G1-phase Cell Cycle Regulators. *Development* 130 (3), 539–552. doi:10.1242/dev.00275
- Gu, B., and Lee, M. (2013). Histone H3 Lysine 4 Methyltransferases and Demethylases in Self-Renewal and Differentiation of Stem Cells. *Cell Biosci.* 3 (1), 39. doi:10.1186/2045-3701-3-39

- Guido, W. (2018). Development, Form, and Function of the Mouse Visual Thalamus. *J. Neurophysiol.* 120 (1), 211–225. doi:10.1152/jn.00651.2017
- Hafner, B. P., Surzenko, N., Beier, K. T., Punzo, C., Trimarchi, J. M., Kong, J. H., et al. (2012). Transcription Factor Olig2 Defines Subpopulations of Retinal Progenitor Cells Biased toward Specific Cell Fates. *Proc. Natl. Acad. Sci.* 109 (20), 7882–7887. doi:10.1073/pnas.1203138109
- Hennig, A. K., Peng, G.-H., and Chen, S. (2008). Regulation of Photoreceptor Gene Expression by Crx-Associated Transcription Factor Network. *Brain Res.* 1192, 114–133. doi:10.1016/j.brainres.2007.06.036
- Jakovcevski, M., Ruan, H., Shen, E. Y., Dincer, A., Javidfar, B., Ma, Q., et al. (2015). Neuronal Kmt2a/Mll1 Histone Methyltransferase Is Essential for Prefrontal Synaptic Plasticity and Working Memory. *J. Neurosci.* 35 (13), 5097–5108. doi:10.1523/JNEUROSCI.3004-14.2015
- Jones, W. D., Dafou, D., McEntagart, M., Woollard, W. J., Elmslie, F. V., Holder-Espinasse, M., et al. (2012). De Novo mutations in MLL Cause Wiedemann-Steiner Syndrome. *Am. J. Hum. Genet.* 91 (2), 358–364. doi:10.1016/j.ajhg.2012.06.008
- Kerimoglu, C., Sakib, M. S., Jain, G., Benito, E., Burkhardt, S., Capece, V., et al. (2017). KMT2A and KMT2B Mediate Memory Function by Affecting Distinct Genomic Regions. *Cel Rep.* 20 (3), 538–548. doi:10.1016/j.celrep.2017.06.072
- Kim, D. S., Ross, S. E., Trimarchi, J. M., Aach, J., Greenberg, M. E., and Cepko, C. L. (2008). Identification of Molecular Markers of Bipolar Cells in the Murine Retina. *J. Comp. Neurol.* 507 (5), 1795–1810. doi:10.1002/cne.21639
- Koike, C., Nishida, A., Ueno, S., Saito, H., Sanuki, R., Sato, S., et al. (2007). Functional Roles of Otx2 Transcription Factor in Postnatal Mouse Retinal Development. *Mol. Cell Biol.* 27 (23), 8318–8329. doi:10.1128/MCB.01209-07
- Krivtsov, A. V., and Armstrong, S. A. (2007). MLL Translocations, Histone Modifications and Leukaemia Stem-Cell Development. *Nat. Rev. Cancer* 7 (11), 823–833. doi:10.1038/nrc2253
- Le, Y. Z., Ash, J. D., Al-Ubaidi, M. R., Chen, Y., Ma, J. X., and Anderson, R. E. (2004). Targeted Expression of Cre Recombinase to Cone Photoreceptors in Transgenic Mice. *Mol. Vis.* 10, 1011–1018.
- Li, B., Carey, M., and Workman, J. L. (2007). The Role of Chromatin during Transcription. *Cell* 128 (4), 707–719. doi:10.1016/j.cell.2007.01.015
- Liu, I. S. C., Chen, J.-d., Ploder, L., Vidgen, D., van der Kooy, D., Kalnins, V. I., et al. (1994). Developmental Expression of a Novel Murine Homeobox Gene (Chx10): Evidence for Roles in Determination of the Neuroretina and Inner Nuclear Layer. *Neuron* 13 (2), 377–393. doi:10.1016/0896-6273(94)90354-9
- Livesey, F. J., and Cepko, C. L. (2001). Vertebrate Neural Cell-Fate Determination: Lessons from the Retina. *Nat. Rev. Neurosci.* 2 (2), 109–118. doi:10.1038/35053522
- Livne-bar, I., Pacal, M., Cheung, M. C., Hankin, M., Trogadis, J., Chen, D., et al. (2006). Chx10 Is Required to Block Photoreceptor Differentiation but Is Dispensable for Progenitor Proliferation in the Postnatal Retina. *Proc. Natl. Acad. Sci.* 103 (13), 4988–4993. doi:10.1073/pnas.0600083103
- Lu, Y., Shiau, F., Yi, W., Lu, S., Wu, Q., Pearson, J. D., et al. (2020). Single-Cell Analysis of Human Retina Identifies Evolutionarily Conserved and Species-Specific Mechanisms Controlling Development. *Dev. Cel.* 53 (4), 473–491. e479. doi:10.1016/j.devcel.2020.04.009
- Mears, A. J., Kondo, M., Swain, P. K., Takada, Y., Bush, R. A., Saunders, T. L., et al. (2001). Nrl Is Required for Rod Photoreceptor Development. *Nat. Genet.* 29, 447–452. doi:10.1038/ng774
- Mellough, C. B., Bauer, R., Collin, J., Dorgau, B., Zerti, D., Dolan, D. W. P., et al. (2019). An Integrated Transcriptional Analysis of the Developing Human Retina. *Development* 146 (2), dev169474. doi:10.1242/dev.169474
- Meyers, R. M., Bryan, J. G., McFarland, J. M., Weir, B. A., Sizemore, A. E., Xu, H., et al. (2017). Computational Correction of Copy Number Effect Improves Specificity of CRISPR-Cas9 Essentiality Screens in Cancer Cells. *Nat. Genet.* 49 (12), 1779–1784. doi:10.1038/ng.3984
- Milne, T. A., Briggs, S. D., Brock, H. W., Martin, M. E., Gibbs, D., Allis, C. D., et al. (2002). MLL Targets SET Domain Methyltransferase Activity to Hox Gene Promoters. *Mol. Cell.* 10 (5), 1107–1117. doi:10.1016/S1097-2765(02)00741-4
- Morrow, E. M., Chen, C.-M. A., and Cepko, C. L. (2008). Temporal Order of Bipolar Cell Genesis in the Neural Retina. *Neural Dev.* 3 (1), 2. doi:10.1186/1749-8104-3-2
- Nadal-Nicola's, F. M., Jimé'nez-Lo'pez, M., Sobrado-Calvo, P., Nieto-Lo'pez, L., Ca'novas-Marti'nez, I., Salinas-Navarro, M., et al. (2009). Brn3a as a Marker of Retinal Ganglion Cells: Qualitative and Quantitative Time Course Studies in Naïve and Optic Nerve-Injured Retinas. *Invest. Ophthalmol. Vis. Sci.* 50 (8), 3860–3868. doi:10.1167/iovs.08-3267
- Nishida, A., Furukawa, A., Koike, C., Tano, Y., Aizawa, S., Matsuo, I., et al. (2003). Otx2 Homeobox Gene Controls Retinal Photoreceptor Cell Fate and Pineal Gland Development. *Nat. Neurosci.* 6 (12), 1255–1263. doi:10.1038/nn1155
- Remez, L. A., Onishi, A., Menuchin-Lasowski, Y., Biran, A., Blackshaw, S., Wahlin, K. J., et al. (2017). Pax6 Is Essential for the Generation of Late-Born Retinal Neurons and for Inhibition of Photoreceptor-Fate during Late Stages of Retinogenesis. *Dev. Biol.* 432 (1), 140–150. doi:10.1016/j.ydbio.2017.09.030
- Roberts, M. R., Hendrickson, A., McGuire, C. R., and Reh, T. A. (2005). Retinoid X Receptor γ Is Necessary to Establish the S-Opsin Gradient in Cone Photoreceptors of the Developing Mouse Retina. *Invest. Ophthalmol. Vis. Sci.* 46 (8), 2897–2904. doi:10.1167/iovs.05-0093
- Roberts, M. R., Srinivas, M., Forrest, D., Morreale de Escobar, G., and Reh, T. A. (2006). Making the Gradient: Thyroid Hormone Regulates Cone Opsin Expression in the Developing Mouse Retina. *Proc. Natl. Acad. Sci.* 103 (16), 6218–6223. doi:10.1073/pnas.0509981103
- Rowan, S., and Cepko, C. L. (2004). Genetic Analysis of the Homeodomain Transcription Factor Chx10 in the Retina Using a Novel Multifunctional BAC Transgenic Mouse Reporter. *Dev. Biol.* 271 (2), 388–402. doi:10.1016/j.ydbio.2004.03.039
- Ruzycki, P. A., Zhang, X., and Chen, S. (2018). CRX Directs Photoreceptor Differentiation by Accelerating Chromatin Remodeling at Specific Target Sites. *Epigenetics Chromatin* 11 (1), 42. doi:10.1186/s13072-018-0212-2
- Sapkota, D., Chintala, H., Wu, F., Fliesler, S. J., Hu, Z., and Mu, X. (2014). Onecut1 and Onecut2 Redundantly Regulate Early Retinal Cell Fates during Development. *Proc. Natl. Acad. Sci. USA* 111 (39), E4086–E4095. doi:10.1073/pnas.1405354111
- Shilatifard, A. (2008). Molecular Implementation and Physiological Roles for Histone H3 Lysine 4 (H3K4) Methylation. *Curr. Opin. Cell Biol.* 20 (3), 341–348. doi:10.1016/j.ceb.2008.03.019
- Shinsky, S. A., Monteith, K. E., Viggiano, S., and Cosgrove, M. S. (2015). Biochemical Reconstitution and Phylogenetic Comparison of Human SET1 Family Core Complexes Involved in Histone Methylation. *J. Biol. Chem.* 290 (10), 6361–6375. doi:10.1074/jbc.M114.627646
- Slany, R. K. (2016). The Molecular Mechanics of Mixed Lineage Leukemia. *Oncogene* 35 (40), 5215–5223. doi:10.1038/onc.2016.30
- Soto, F., Ma, X., Cecil, J. L., Vo, B. Q., Culican, S. M., and Kerschensteiner, D. (2012). Spontaneous Activity Promotes Synapse Formation in a Cell-Type-dependent Manner in the Developing Retina. *J. Neurosci.* 32 (16), 5426–5439. doi:10.1523/JNEUROSCI.0194-12.2012
- Stenkamp, D. L. (2015). Development of the Vertebrate Eye and Retina. *Prog. Mol. Biol. Transl. Sci.* 134, 397–414. doi:10.1016/bs.pmbts.2015.06.006
- Swaroop, A., Kim, D., and Forrest, D. (2010). Transcriptional Regulation of Photoreceptor Development and Homeostasis in the Mammalian Retina. *Nat. Rev. Neurosci.* 11, 563–576. doi:10.1038/nrn2880
- Szatko, K. P., Korympidou, M. M., Ran, Y., Berens, P., Dalkara, D., Schubert, T., et al. (2020). Neural Circuits in the Mouse Retina Support Color Vision in the Upper Visual Field. *Nat. Commun.* 11 (1), 3481. doi:10.1038/s41467-020-17113-8
- Sze, C. C., and Shilatifard, A. (2016). MLL3/MLL4/COMPASS Family on Epigenetic Regulation of Enhancer Function and Cancer. *Cold Spring Harb Perspect. Med.* 6 (11), a026427. doi:10.1101/cshperspect.a026427
- Tian, N. (2004). Visual Experience and Maturation of Retinal Synaptic Pathways. *Vis. Res.* 44 (28), 3307–3316. doi:10.1016/j.visres.2004.07.041
- Tran, N. M., Zhang, A., Zhang, X., Huecker, J. B., Hennig, A. K., and Chen, S. (2014). Mechanistically Distinct Mouse Models for CRX-Associated Retinopathy. *Plos Genet.* 10 (2), e1004111. doi:10.1371/journal.pgen.1004111
- Turner, D. L., Snyder, E. Y., and Cepko, C. L. (1990). Lineage-independent Determination of Cell Type in the Embryonic Mouse Retina. *Neuron* 4 (6), 833–845. doi:10.1016/0896-6273(90)90136-4
- Wu, F., Li, R., Umino, Y., Kaczynski, T. J., Sapkota, D., Li, S., et al. (2013). Onecut1 Is Essential for Horizontal Cell Genesis and Retinal Integrity. *J. Neurosci.* 33 (32), 13053–13065. doi:10.1523/JNEUROSCI.0116-13.2013
- Wu, S., Chang, K.-C., and Goldberg, J. L. (2018). Retinal Cell Fate Specification. *Trends Neurosci.* 41 (4), 165–167. doi:10.1016/j.tins.2018.02.002
- Yokoyama, A., Wang, Z., Wsocka, J., Sanyal, M., Aufiero, D. J., Kitabayashi, I., et al. (2004). Leukemia Proto-Oncoprotein MLL Forms a SET1-like Histone

- Methyltransferase Complex with Menin To Regulate Hox Gene Expression. *Mol. Cell. Biol.* 24 (13), 5639–5649. doi:10.1128/MCB.24.13.5639-5649.2004
- Young, R. W. (1985). Cell Differentiation in the Retina of the Mouse. *Anat. Rec.* 212 (2), 199–205. doi:10.1002/ar.1092120215
- Yu, B. D., Hess, J. L., Horning, S. E., Brown, G. A. J., and Korsmeyer, S. J. (1995). Altered Hox Expression and Segmental Identity in Mll-Mutant Mice. *Nature* 378 (6556), 505–508. doi:10.1038/378505a0
- Zhang, T., Cooper, S., and Brockdorff, N. (2015). The Interplay of Histone Modifications - Writers that Read. *EMBO Rep.* 16 (11), 1467–1481. doi:10.15252/embr.201540945

Conflict of Interest: The authors declare that the research was conducted in the absence of any commercial or financial relationships that could be construed as a potential conflict of interest.

Publisher's Note: All claims expressed in this article are solely those of the authors and do not necessarily represent those of their affiliated organizations, or those of the publisher, the editors and the reviewers. Any product that may be evaluated in this article, or claim that may be made by its manufacturer, is not guaranteed or endorsed by the publisher.

Copyright © 2022 Sun, Zhang, Ruzycski and Chen. This is an open-access article distributed under the terms of the Creative Commons Attribution License (CC BY). The use, distribution or reproduction in other forums is permitted, provided the original author(s) and the copyright owner(s) are credited and that the original publication in this journal is cited, in accordance with accepted academic practice. No use, distribution or reproduction is permitted which does not comply with these terms.